Broadband photonic crystal antireflection

M. Malekmohammad
malek46@gmail.com

Department of Physics, Faculty of science, University of Isfahan, Hezar Jerib, 81746-73441, Isfahan, Iran

M. Soltanolkotabi

Department of Physics, Faculty of science, University of Isfahan, Hezar Jerib, 81746-73441, Isfahan, Iran

A. Erfanian

Department of Electrical Engineering, K.N. Toosi University of Technology, Seyyed Khandan Bridge, Tehran, Iran

R. Asadi

Department of Physics, University of Tehran, Kargar Street, Tehran, Iran

S. Bagheri

Laser and Plasma Research Institute, Shahid Beheshti University - G.C. Evin, Tehran, Iran

M. Zahedinejad

Department of Electrical Engineering, K.N. Toosi University of Technology, Seyyed Khandan Bridge, Tehran, Iran

M. Khaje

Department of Electrical Engineering, K.N. Toosi University of Technology, Seyyed Khandan Bridge, Tehran, Iran

M. H. Naderi

Department of Physics, Faculty of science, University of Isfahan, Hezar Jerib, 81746-73441, Isfahan, Iran

Broadband antireflection layers have been fabricated by two dimensional (2D) photonic crystals (PCs) with tapered pillars on the Si substrate. These PCs have been produced by interference lithography and reactive ion etching (RIE) techniques. The effect of depth and the filling factor (FF) of the PCs on the reflectance magnitude and bandwidth has been investigated. The obtained reflectance was less than 1% in the broad spectral range from 400 to 2100 nm. Our numerical simulation shows the PC pillars slope has an essential effect in the reduction of the reflection. However, our results show that the existence of RIE grasses in the PCs, which are created in the RIE process, does not influence the performance of the antireflection layer. This leads to a simpler fabrication process. [DOI: http://dx.doi.org/10.2971/jeos.2012.12008]

Keywords: photonic crystal, interference lithography, antireflection

1 INTRODUCTION

Fabrication of antireflection layer in many optical sensors such as solar cells and photo detectors is an interesting subject for many investigators [1]–[6]. This is especially important for silicon-based devices that have a high refractive index and thus high reflectance [7, 8]. There are several methods to decrease the reflectance of these devices such as manufacturing antireflection single layer [9] or multiple layers [10]. In the antireflection single layer the reflection reduction occurs only in a narrow spectral range where as in multiple antireflection layers, the limitation is choosing suitable material to obtain a large spectral width.

Another method for the reduction of the reflectance in these devices is using pores to produce intermediate antireflection layers with suitable refractive index matching between the air and the substrate [11]–[15]. Recently, moth eye structure has been used as an antireflection layer in wide bandwidths [16]–[18]. This structure is a 2D random array of tapered pillars with a sub-wavelength mean period. These structures have good antireflection performance due to gradual increase the effective refractive index which leads to suitable index matching.

Periodic structures or PCs have also been utilized as an antireflection layer. PCs can excite multiple resonances and enhance the absorption in photovoltaic applications. Moreover in comparison with the moth eye structure PCs are more architectable. But it is difficult to fabricate high quality large area 2D tapered pillars. In addition the existence of multiple resonances cause of non-uniformity in reflection spectrum. We recently present a new method to fabricate an antireflection layer based on the combination of hole array PCs and nanoporous structures [19].

In this paper, we have used a simple and cost-efficient fabrication method by interface lithography and single step RIE techniques to produce large area 2D tapered PC as an antireflection layer. We show that the existence of the undesirable artifact cones around the PC pillars (RIE grasses) which occurs in the RIE process does not affect its performance but reduces the non-uniformity in the reflection spectrum. Moreover, we
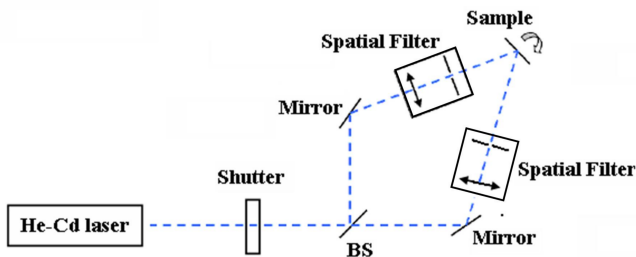
FIG. 1 Schematic of interference lithography setup used for fabrication of photonic Crystals.

find that the existence of a small slope in the PC pillars side-walls has an essential effect on the reflection reduction.

2 Experiment

As mentioned above, we have fabricated 2D Si PCs by interference lithography and Reactive Ion Etching (RIE) techniques. Schematic setup of the interference lithography is shown in Figure 1 .We have used a He-Cd laser with 325 nm wavelength. The laser beam was split by a beam splitter (BS) into two beams of equal intensity and passed through two spatial filters to delete speckles. The divided beams were directed toward the sample to interfere with each other in the photoresist layer coated on the sample. The period of the interference pattern is given by $a = \lambda/2 \sin(\theta/2)$, where λ and θ are the laser wavelength and the angle between the beams, respectively. In order to produce 2D PC, after the first irradiation step, the sample is rotated 90 degrees and irradiated again. The sample was composed of Si substrate coated by a 50 nm Cr layer and Shipley S1400 photoresist. At this stage we created the PC pattern on the photoresist, and then the pattern was transferred to the Cr layer by chemical wet etching. The Cr layer was used as a mask. Then the Si substrate was etched by the RIE method and finally the Cr and photoresist layers were removed. We have measured the reflectance spectra (R) of the PCs by using a Horiba Jobin Yvon Ellipsometer.

3 Results

We have fabricated various 2D PCs with the same periods of 1.3 μm and the same etch depth but with different FF to investigate the effect of FF on the reflectance. Figure 2 and Figure 3 show the results for PCs with depth of 2.6 μm and 4.2 μm respectively. Figure 2(a) and Figure 2(b) show SEM images of PCs with low FF (0.1) and high FF (0.3) respectively. Figure 2(c) shows the reflectance spectra of these samples. This Figure shows that the reflection reduces to lower magnitudes when FF increases. In other words, by increasing FF from 0.1 to 0.3 the average reflectance decreases from 13% to 4% in the wavelength range of 400 nm to 1600 nm.

The same behavior of reflectance spectra was obtained for PCs with a higher depth of 4.2 μm as shown in Figure 3. Figure 3(a) and Figure 3(b) show SEM images of PCs with low FF (0.1) and high FF (0.3) respectively. Figure 3(c) shows the
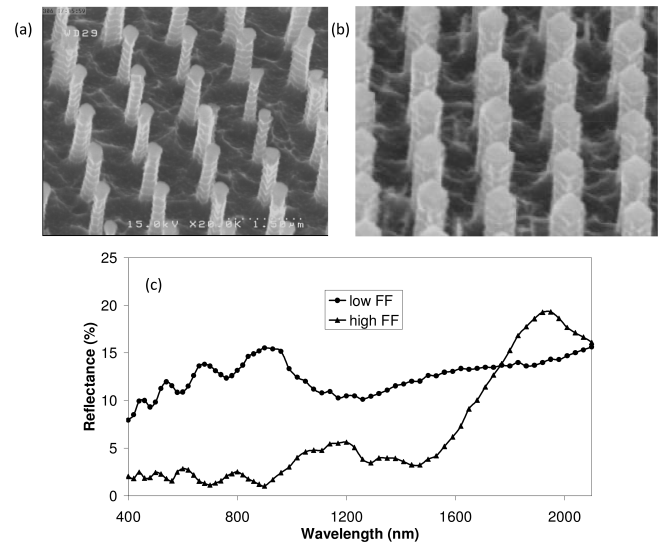

FIG. 2 SEM images of low FF (0.1) (a), and high FF (0.3) (b), PCs with period of 1.3 μm and etch depth of 2.6 μm and (c) Reflectance spectra of PC samples.
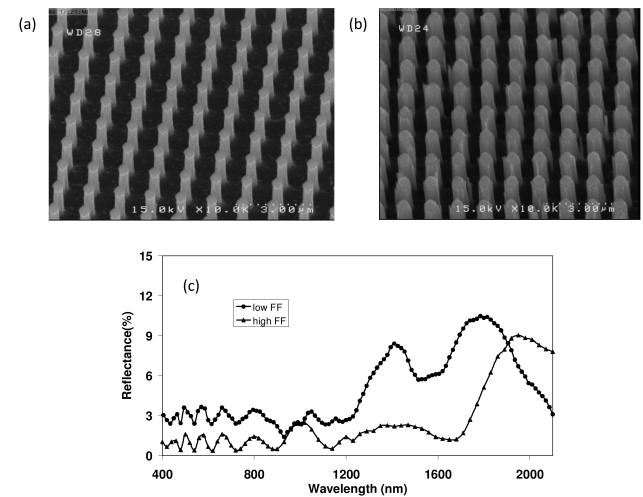

FIG. 3 SEM images of low (0.1) (a), and high (0.3) (b), FF PCs with a period of 1.3 μm and etch depth of 4.2 μm and (c) Reflectance spectra of these PC samples.

reflectance spectra of the corresponding samples. This figure shows that the reflection is reduced to lower magnitudes when FF increases. In other words, FF values from 0.1 to 0.3 drop the average reflectance from approximately 10% to 2% in the wavelength range of 400 nm to 1700 nm. Furthermore, the antireflection bandwidth has expanded up to 1800 nm. In order to investigate the effect of the etch depth of PCs on reflectance we fabricated several PCs with the same periods of 1.3 μm and FF of about 0.3 but with different etch depths ranging from 1.2 μm to 6.6 μm.

Figures 4(a) to 4(d) show SEM images of two samples with 1.2 μm and 6.6 μm depths respectively. In Figure 4(e), the corresponding reflectance spectra for the four different depths from 1.2 μm to 6.6 μm are shown. This Figure shows that by enhancing the PC depth, the magnitude of reflectance decreases and the bandwidth increases. For the depth of 6.6 μm the average reflectance for both P and S polarization is less than 1% in the wavelength range of 400 to 2100 nm which indicates the broadband antireflection behavior. It is worth
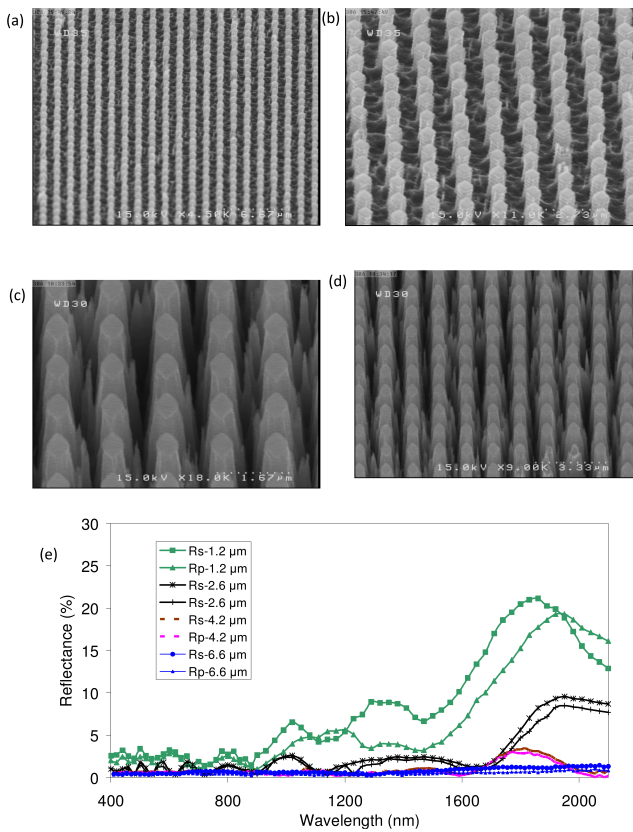
FIG. 4 (a-d) SEM images of the fabricated PCs with period of 1.3 but with different etch depth of 1.2 μm (a-b), and 6.6 μm (c-d), the undesirable artifact cones around the PC pillars are RIE grasses that occur in the RIE process. (e) The corresponding reflectance spectra of the PC samples for etch depth of 1.2 μm, 2 μm, 2.6 μm, 4.2 μm and 6.6 μm and for S and P light polarization

FIG. 5 Comparison of simulated hemispherical reflection spectra in the vertical side-walls and tapered PCs with 6.6 μm depth

FIG. 6 Comparison of reflection spectra for highly ordered tapered PCs and PCs with grass structures simulated by FDTD method and measured reflection spectrum

mentioning that we have measured the overall reflection (non- specula) for all wavelengths and it turned out to be less than 1%.

4 Simulation and Discussion

Hemispherical reflection (including specular reflection, diffraction and scattering) for a PC of 6.6 μm depth for both vertical and tapered sidewalls has been simulated using the FDTD method. The slope of the tapered sidewalls is considered 86 degrees that corresponds to the slope of the fabricated sample in Figure 4(c). Figure 5 shows simulated reflectance spectra of these PCs. As can be seen, the tapered PC has a much lower reflection and also lower fluctuation in comparison with PC with vertical sidewalls. Furthermore, the reflectance of the tapered PC is comparable with the measurement result (blue curve in Figure 4(e)).

In Figure 5 the fluctuations in PCs with vertical sidewalls are due to light resonance and light surface coupling that come from the PC modes. In tapered PC, the bandwidth of the PC modes is increased due to the decreasing of the quality factor of the PC. This effect decreases the fluctuations of the reflectance. In addition, the existence of the grasses (undesirable cones) around the PC pillars that are observed
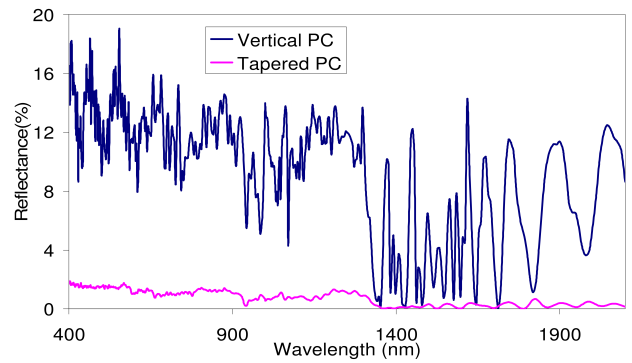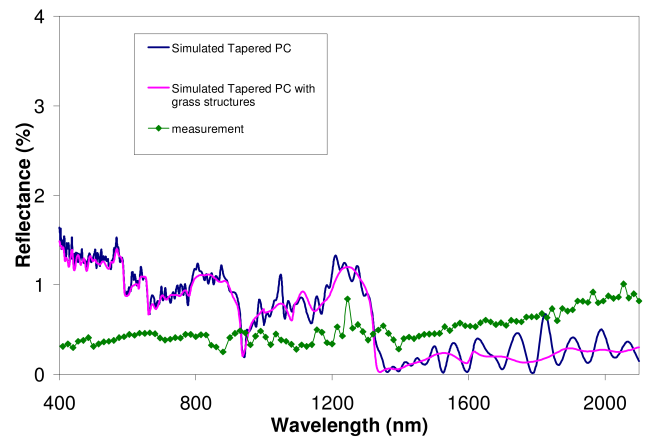
in the fabricated PC with 6.6 μm depth in Figures 4(c) and 4(d), decrease the PC quality factor moreover. These grasses are made in the RIE process. To consider the effect of these grasses in the reflectance we added conical pillars with random height (in the range of 0 to 6.6 μm) and base diameter (in the range of 0 to 100 nm) in the tapered PC structure simulated in Figure 5. The result has been shown in Figure 6 and compared with the measurement. Also for comparison, in this Figure we plot again the results of calculated tapered PC without grass. It is obvious that the existence of the grasses decreases the spectrum fluctuations and has not influence on the average of the reflectance.

To improve our understanding of the obtained results, we calculated the reflectance of the fabricated sample using the FDTD method and index matching model. In this model, the textured layer is considered as a slab with gradually increasing effective refractive index that is calculated by $n_e(h) = n_{si}FF(h) + 1 - FF(h)$, where n_{si} is the refractive index of the Si and $FF(h)$ is the filling factor of Si in the depth of h. The calculated reflectance for the fabricated tapered PC with 6.6 μm depth and its effective refractive index are shown in Figures 7(a) and 7(b). As can be seen in Figure 7(b), there are two sharp changes in the effective refractive index corresponding to the top and bottom of the slab. The multiple reflections from the top and bottom surfaces of the slab cause fluctuations in the reflectance. We have also shown the re-
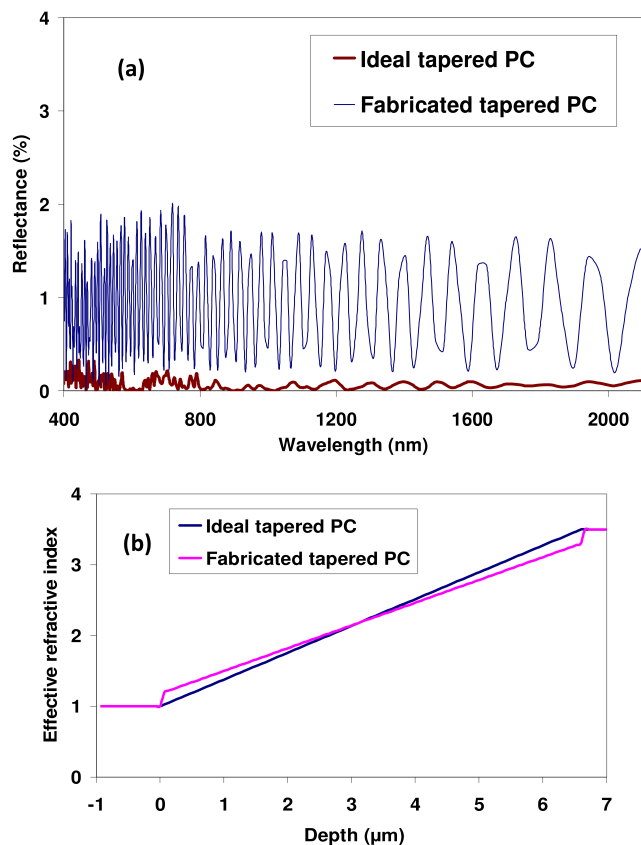
FIG. 7 The calculated reflectance for the fabricated and ideal tapered PC with 6.6 μm depth (a) and the effective refractive index as a function of depth (b).

flectance of the slab if the refractive effective index were to gradually change in both the top and bottom of the slab (Figure 7(b), blue lines).This corresponds to an ideal tapered PC as shown in Figure 7(a). As demonstrated in this case, the reflectance is reduced to near zero. By referring to the results of the index matching model in Figure 7(a) and to the corresponding simulated and measured results indicated in Figure 6, it is obvious that the index matching effect has major contribution to the reflection reduction and PC modes may only cause some fluctuations predicted by the index matching model.

5 Conclusion

We investigated the effect of depth and FF of PCs in Si substrate. We have significantly improved the reduction of reflectance and enhancement of the bandwidth in our samples. In other words, increasing the etch depth and FF reduces the reflectance. We have also found the reflection reduction for both P and S incident light polarizations. The reflection of our PC with 6.6 μm depth and 86 degrees side wall slopes, on average, is less than 1% in the wavelength range of 400nm to 2100 nm. This reduction in reflectance is significantly lower than the corresponding one in bare Si which is more than 30%. By comparing the experimental curve and the corresponding simulated curve, we found that even poor quality PC with the presence of grasses generated low reflection. Moreover, tapering the PCs pillars further reduces the reflection in the wide bandwidth. We believe that due to lower reflections, our sam-

ple may enhance the efficiency of solar cells and photodetectors.

References

[1] J. Bae, H. Kim, X. M. Zhang, C. H. Dang, Y. Zhang, Y. Jin Choi, A. Nurmikko, and Z. Lin Wang, "Si nanowire metal-insulator-semiconductor photodetectors as efficient light harvesters," Nanotechnology **21**, 095502 (2010).

[2] J. Chen, Q. Wang, and H. Li, "Microstructured design for light trapping in thin-film silicon solar cells," Opt. Eng. **49**, 088001 (2010).

[3] H. C. Lee, S. C. Wu, T. C. Yang, and T. J. Yen, "Efficiently Harvesting Sun Light for Silicon Solar Cells through Advanced Optical Couplers and A Radial pn Junction Structure," Energies **3**, 784–802 (2010).

[4] Y. Park, E. Drouard, O. El Daif, X. Letartre, P. Viktorovitch, A. Fave, A. Kaminski, M. Lemiti, and C. Seassal, "Absorption enhancement using photonic crystals for silicon thin film solar cells," Opt. Express **17**, 14312–21 (2009).

[5] Y. J. Hung, S. L. Lee, and L. A. Coldren, "Deep and tapered silicon photonic crystals for achieving anti-reflection and enhanced absorption," Opt. Express **18**, 6841–52 (2010).

[6] A. Chutinan, N. P. Kherani, and S. Zukotynski, "High-efficiency photonic crystal solar cell architecture," Opt. Express **17**, 8871-8 (2009).

[7] Y. M. Song, J. S. Yu, and Y. T. Lee, "Antireflective submicrometer gratings on thin-film silicon solar cells for light-absorption enhancement," Opt. Lett. **35**, 276-8 (2010).

[8] C. Morhard, C. Pacholski, D. Lehr, R. Brunner, M. Helgert, M. Sundermann, and J. P. Spatz, "Tailored antireflective biomimetic nanostructures for UV applications," Nanotechnology **21**, 425301 (2010).

[9] F. Zhan, H. L. Wang, J. F. He, J. Wang, S. S. Huang, H. Q. Ni, and Z. C. Niu, "Multilayer Antireflection Coating for Triple Junction Solar Cells," Chinese Phys. Lett. **28**, 047802 (2011).

[10] A. Chutinan, N. P. Kherani, and S. Zukotynski, "High-efficiency photonic crystal solar cell architecture," Opt. Express **17**, 8871-8 (2009).

[11] J. Q. Xi, M. F. Schubert, J. K. Kim, E. F. Schubert, M. Chen, S. Y. Lin, W. Liu, and J. A. Smart, "Optical thin-film materials with low refractive index for broadband elimination of Fresnel reflection," Nat. Photonics **1**, 176-9 (2007).

[12] J. Kim, "Formation of a Porous Silicon Anti-Reflection Layer for a Silicon Solar Cell," J. Korean Phys. Soc. **50**, 1168 (2007).

[13] F. Duerinckx, I. Kuzma-Filipek, K. Van Nieuwenhuysen, G. Beaucarne, and J. Poortmans, "Simulation and implementation of a porous silicon reflector for epitaxial silicon solar cells," Prog. Photovoltaics **16**, 399-407 (2008).

[14] C. H. Chang, P. Yu, M. H. Hsu, P. C. Tseng, W. L. Chang, W. C. Sun, W. C. Hsu, S. H. Hsu, and Y. C. Chang, "Combined micro-and nano-scale surface textures for enhanced near-infrared light harvesting in silicon photovoltaics," Nanotechnology **22**, 095201 (2011).

[15] C. C. Striemer, and P. M. Fauchet, "Dynamic etching of silicon for broadband antireflection applications," Appl. Phys. Lett. **81**, 2980

(2002).

[16] C. H. Sun, P. Jiang, and B. Jiang, "Broadband moth-eye antireflection coatings on silicon," Appl. Phys. Lett. **92**, 061112 (2008).

[17] Y. F. Huang, S. Chattopadhyay, Y. J. Jen, C. Y. Peng, T. A. Liu, Y. K. Hsu, C. L. Pan, H. C. Lo, C. H. Hsu, Y. H. Chang, and others, "Improved broadband and quasi-omnidirectional anti-reflection properties with biomimetic silicon nanostructures," Nat. Nanotechnol. **2**, 770–4 (2007).

[18] S. A. Boden, and D. M. Bagnall, "Optimization of moth-eye antireflection schemes for silicon solar cells," Prog. Photovoltaics **18**, 195–203 (2010).

[19] M. Malekmohammad, M. Soltanolkotabi, A.Erfanian, R. Asadi,; M. Zahedinejad, S. Bagheri, and M. Khaje, "Hybrid structure for efficiency enhancement of photodetectors," submitted to Appl. Surf. Sci.